AFRL-SR-AR-TR-10-0205

REPORT DOCUMENTATION PAGE

PLEASE DO NOT RETURN YOUR FORM TO THE ABOVE ORGANIZATION.

1. REPORT DATE *(DD-MM-YYYY)*	2. REPORT TYPE	3. DATES COVERED *(From - To)*
31-01-2010	Final	Oct 24,2007 to Jan 31, 2010

4. TITLE AND SUBTITLE
Combustion stability innovations for liquid rocket

5a. CONTRACT NUMBER
FA9550-08-C-0014

5b. GRANT NUMBER

5c. PROGRAM ELEMENT NUMBER

6. AUTHOR(S)
Sampath Palaniswamy and Vigor Yang

5d. PROJECT NUMBER

5e. TASK NUMBER

5f. WORK UNIT NUMBER

7. PERFORMING ORGANIZATION NAME(S) AND ADDRESS(ES)
Metacomp Technologies, Inc., 28632 Roadside Drive, #255, Agoura Hills, CA 91301
Georgia Institute of Technology, 313 Montgomery Knight Building, 270 Ferst Drive NW, Atlanta GA 30332

8. PERFORMING ORGANIZATION REPORT NUMBER

9. SPONSORING/MONITORING AGENCY NAME(S) AND ADDRESS(ES)
AFOSR, 875 N Randolph Street, Room 3112, Arlington, VA 22203

10. SPONSOR/MONITOR'S ACRONYM(S)

11. SPONSOR/MONITOR'S REPORT NUMBER(S)

12. DISTRIBUTION/AVAILABILITY STATEMENT
Distribution A: Approved for public release

13. SUPPLEMENTARY NOTES

20100616376

14. ABSTRACT
Predicting instabilities in liquid rocket engines requires the ability to simulate unsteady reacting flows at high pressures. Intake manifolds, injector design and placement, addition of baffles and acoustic cavities add to the complexity and size of the computational problem at hand. The current effort is focused on the improvement of the basic building blocks which make up the simulation tool. The ability of the toll to track acoustic waves in a low Mach number, unsteady flow with chemical reactions was demonstrated.

15. SUBJECT TERMS
Liquid rocket engine, low-Mach number flows, unsteady flow simulation

16. SECURITY CLASSIFICATION OF:			17. LIMITATION OF ABSTRACT	18. NUMBER OF PAGES	19a. NAME OF RESPONSIBLE PERSON
a. REPORT	b. ABSTRACT	c. THIS PAGE			Sampath Palaniswamy
U	U	U	SAR	23	19b. TELEPHONE NUMBER *(Include area code)* 818 735 4880 ext 231

Liquid Rocket Engine Combustion Instability
FA9550-08-C-0014

Flow instabilities in rocket engines are triggered by the coupling between turbulence, flame fronts and acoustic waves. The ability to resolve scales of turbulence which affect the instability, tracking acoustic wave motions, capturing flame fronts and their interaction with turbulent eddies are required to numerically predict the onset of the instability and its limit-cycle amplitude and frequency. This report summarizes the developments at Metacomp Technologies geared towards rocket engine flow simulation. The focus of the current effort and how it fits in the overall goal of developing an accurate unsteady flow simulation capability is discussed below. Summary of the effort at Metacomp is followed by the research at Penn State and Georgia Tech.

Efforts and Accomplishments at Metacomp Technologies, Inc.

Resolution of acoustic waves in low-speed flows

Modern CFD methods are built on upwinding the inertia terms in the equations. Upwinding provides a systematic way of adding just enough numerical diffusion to prevent oscillations in the flow variables. Upwinding requires knowledge of the local waves speeds. When all the waves in the system are accounted for, numerical diffusion couples all the variables. This is also referred to as matrix diffusion. The main advantage of this strategy is the lack of tuning parameters. However two undesirable effects show up in low speed flow simulation. Firstly, the acoustic speed which is much large than the flow speed dictates the size of the time step that can be taken within an explicit time update. Since the flow velocity is much smaller, a large number of much smaller time steps will have to be computed before any significant changes in the flow field can be detected. It is possible to overcome this with an implicit time update procedure. The second more detrimental effect arises from matrix diffusion proportional to the acoustic speed which dwarfs the flow speed on some components of the flow. The overwhelming diffusion contaminates the momentum equations. This translates to a fourth difference smoothing proportional to the acoustic speed on the velocity field.

Preconditioning methods were developed to alleviate these two difficulties. Artificially lowering the speed of sound in the medium allows for a larger time step while simultaneously reducing the numerical diffusion that affects low speed flow simulation with the conservation form of the equations. While preconditioning works well for steady flow simulation, a dual time stepping scheme is necessary for transient flow simulation where tracking acoustic waves in time is critical to estimating flow dynamics as in a rocket engine. In the dual time stepping scheme, the conservation equations

$$\Gamma \frac{\partial P}{\partial \tau} = -\left\{ \frac{\partial Q}{\partial t} + \nabla \cdot F \right\}$$

Q and P refer to the conservation and primitive variables, respcetively. Γ is the preconditioning matrix. Convergence in pseudo time τ satisfies the unsteady form of the

conservation equations. This approach is consistent with acoustic propagation. However in practice the acoustic waves are heavily damped even with the dual time stepping strategy. A new limiter was developed to control pressure damping which is based on local mesh sizing. If the local mesh size is too large for a given time step size the preconditioning parameter is limited to prevent excessive smoothing of pressure waves.

The following figure shows the geometry of the test case used to assess the ability of the methodology to predict acoustic modes in a pipe open at the left end. An oscillating boundary at the open end generates standing waves within the pipe.

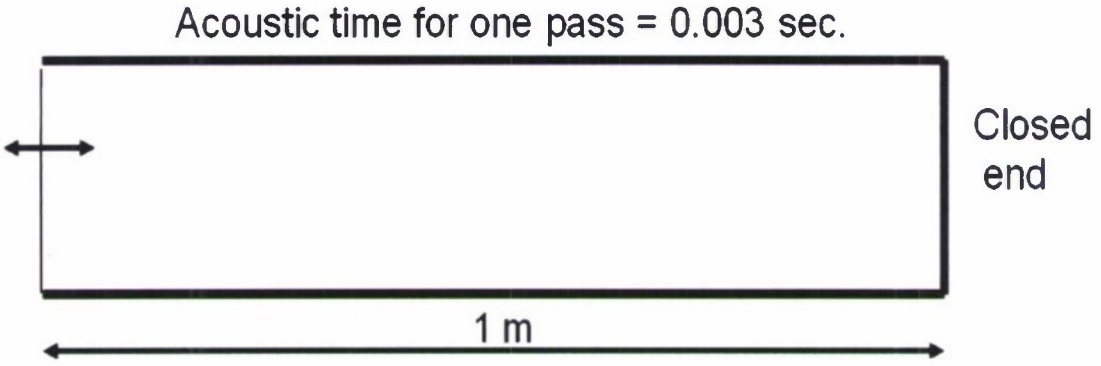

The following figure shows the second harmonic of the quarter wave mode at different time instances. Excellent agreement is obtained with analytical solutions.

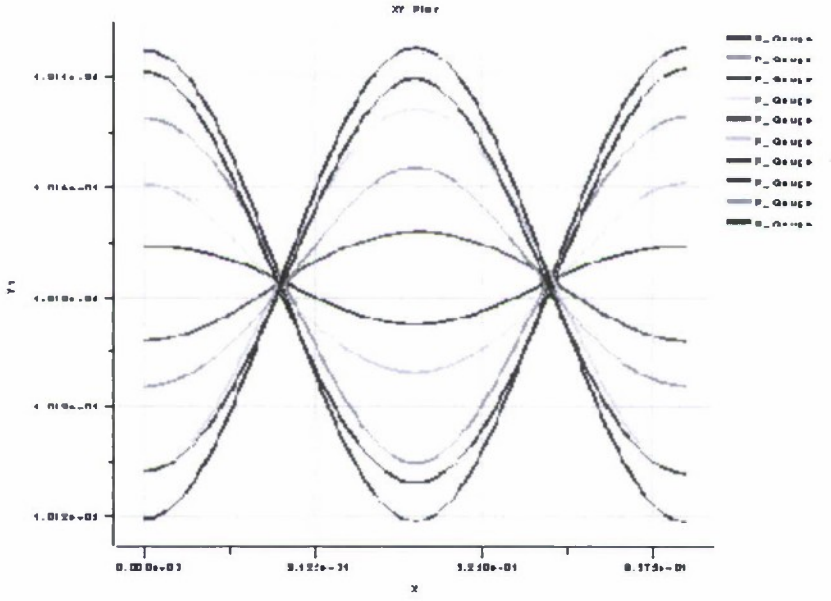

Acoustic Modes in AFRL Combustion Stability Test Rig

Simulations were also conducted to study the acoustic modes in the AFRL Combustion Stability test rig. The acoustic modes in the waveguides were estimated. The following figure shows the pressure wave at 130 Hz.

The mode shape at 2970 Hz is shown below.

In the two cases shown above, the optical windows remained in place. The acoustic pathway is modeled as a continuous channel. The optical windows mesh seamlessly with

the walls of the waveguides at the center of the test section. The two drivers at either end can operate at sync or at a specified phase difference.

The effect of close proximity of the optical windows to the combustion zone was addressed before hot firing the rig. Avoiding the optical sections of the wave guides would be advantageous from the point of view of thermal management. Removing the optical section all together would be desirable but its impact on flow evolution was of concern. The changes in mode shapes without the optical sections were investigated by modeling the entire volume of the test section.

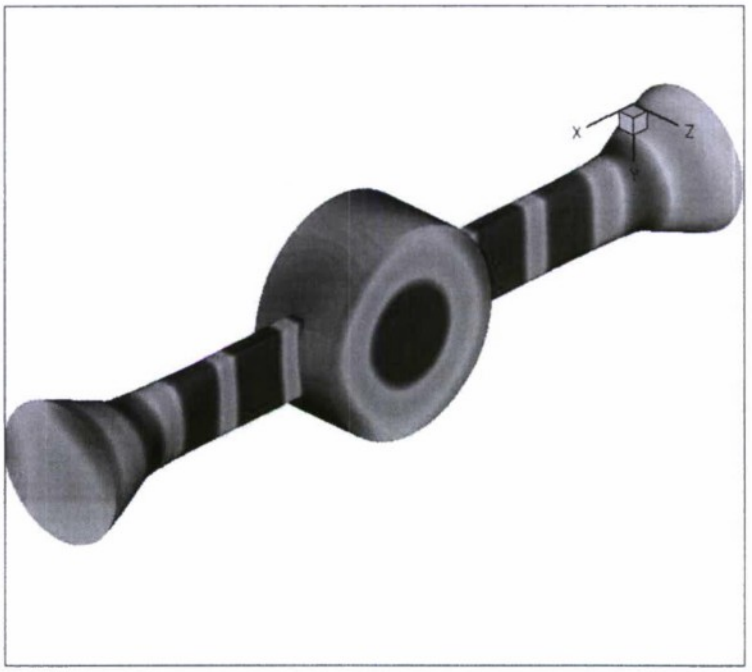

The above figure shows pressure waves at a frequency of 2500 Hz. Modes from 130 Hz to 3000 Hz were obtained to study the chambers response. Quiescent condition at room temperature was assumed in evaluating these modes.

Hybrid RANS/LES (LNS) Methodology for Unsteady Flows

The LNS methodology developed at Metacomp Technologies provides a systematic way of LES. The LNS approach minimizes sub-grid dissipation when the computational mesh gets coarser. The LNS model takes mean flow quantities such turbulence kinetic energy and its dissipation and converts them into a fluctuating field of appropriate frequency when the computation grid is sufficient to resolve these scales. It does not need additional quantities which are difficult to measure at the boundaries to start the calculation. When the grid is sufficiently fine all fluctuation generated by the velocity field are resolved. They are converted to mean flow turbulence quantities only when the mesh is coarse.

Temporal integration

Preeonditioning is eoupled to a dual time stepping seheme to preserve eonservation in real time. The preeonditioner operates on the inner loop driving the solution to the next time level. Sufficient number of inner iterations (< 10) is used to maintain seeond-order time aeeuraey.

Application to a gas-gas combustor

Under a separate effort funded by AFRL, the newly developed algorithm diseussed above, was applied to a 2D eross-seetion of a CH_4-O_2 gas-gas atmospherie pressure test rig[1] to demonstrate the ability to eapture eombustion drive pressure oseillations. The results obtained are related to the methods deseribed above and are presented here for eompleteness. They demonstrate the applieation of the methodology to simulate unsteady reaeting flows.

The inlet geometry was truneated to retain geometrie simplieity. A simple one step ehemieal kinetie meehanism was used in the simulation sinee the goal was to estimate whether the reeent developments to CFD++ eould overeome exeessive pressure damping of preeonditioned systems.

The following figures showing the flow field in the CH_4-O_2 burner. The figure on the left is with eombustion on and shows temperature eontours at an instant of time. These eontours are raised to display pressure waves. When the reaetion was turned off, the pressure oseillations get quieter as shown on the figure to the right. With the eombustion off nearly eireular pressure waves emanate from the injeetor eorresponding to the frequeney at whieh vortiees are shed off. CH4 eontours are used in this figure sinee eombustion is off and temperature remains uniform unlike the reaeting flow shown on the left.

[1] Cavitt, R.C. et. al., "On The Laboratory Scale Survey of Pentad Injector Stability Characteristics", AIAA 2007-5587

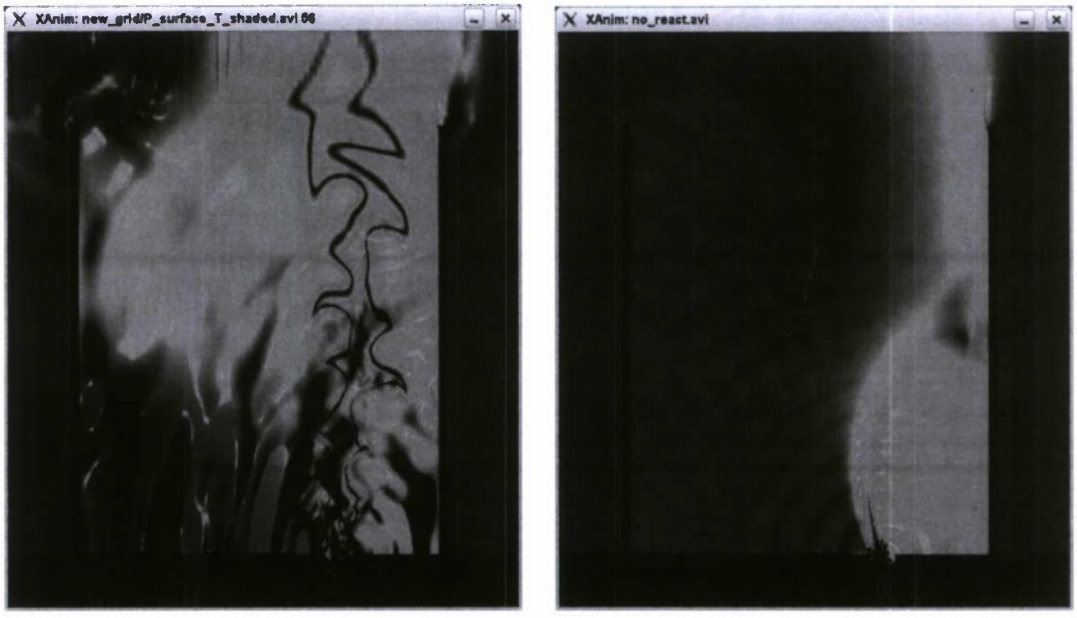

The output from pressure probe inside the combustor is shown below.

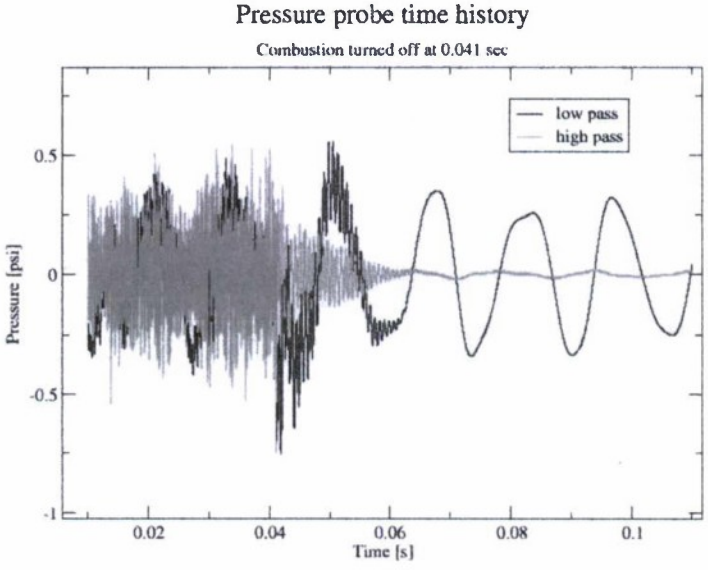

Combustion was turned off at about 0.041 seconds and the green curve in the above figure shows the high frequency content of the pressure tap decay in magnitude without the heat release driving the oscillations. The low frequency oscillations (shown in red) mark bulk sloshing within the chamber at about 70 Hz after the reaction was turned off. Vortex shedding frequency is around 20, 000 Hz with significant amplitude of oscillation when reaction was on. The reaction also drives lower frequencies as shown by the red curve prior to 0.041 seconds.

Heat Load on Wave Guides

The combustor stability test rig at AFRL uses acoustic waves to perturb the fuel jet and study its response to acoustic excitation. Wave guides are used to channel the acoustic energy on to the shear layers formed between the fuel and oxidizer jets. Flow diagnostics is facilitated by using optical windows for the waveguide at the center of the test section. A schematic of the facility is shown below.

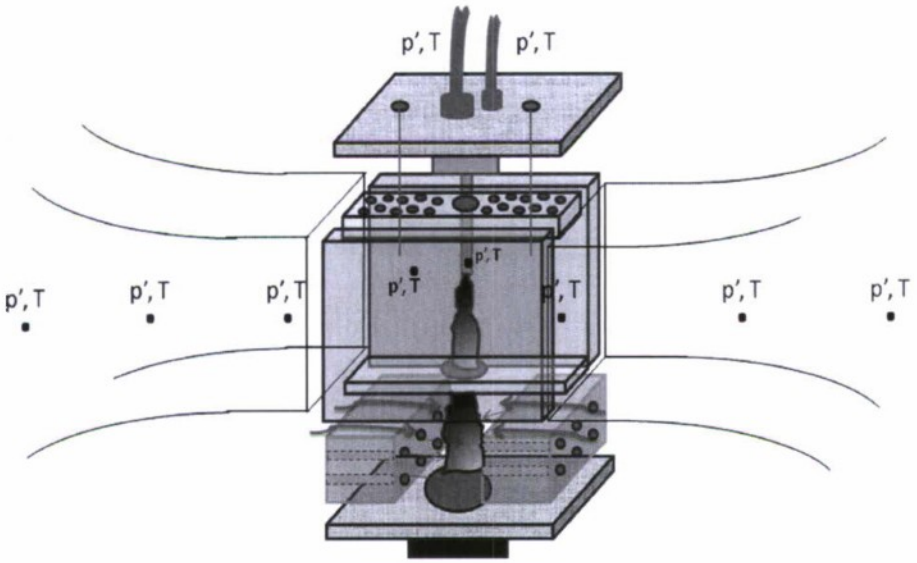

CFD++ was used to study to simulate the flow through the test section. A top view of the flow chamber is shown in the figure below. Only one quarter of the domain shown in red was modeled for computational efficiency since the steady temperature distribution on the wall marked "insulated" in the figure would be a reasonable estimate for the heat load on the optical windows.

CFD++ was used to simulate steady flow in the AFRL test rig. The test facility contains three LOX jets surrounded by annular gaseous H_2 jets. The following figure shows a cross-section of the combustor. The computational domain is shown in red.

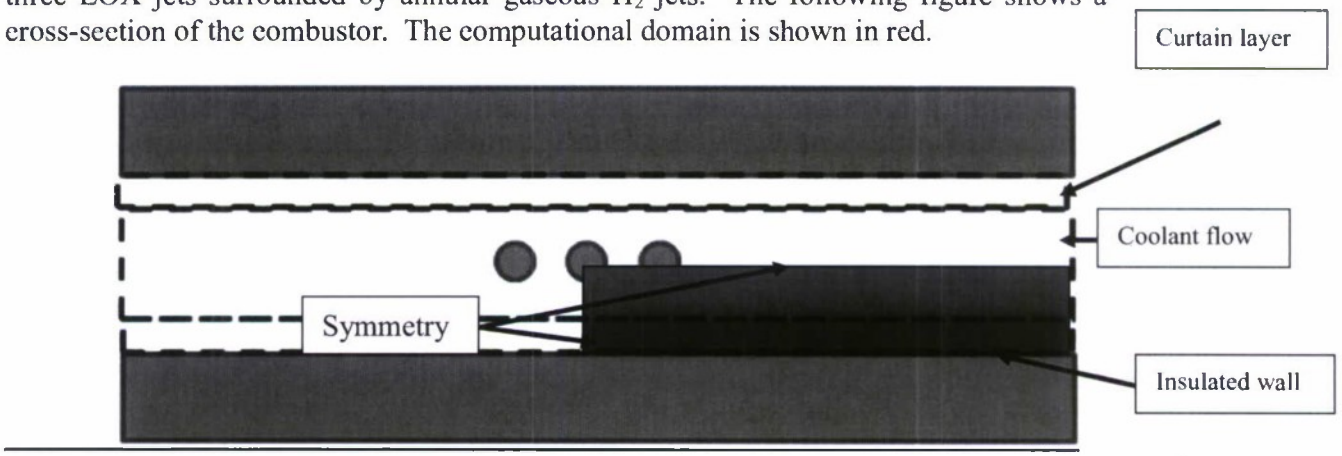

The mass flow rate was specified for the LOX and gaseous H_2 jets. This was run at stoichiometric conditions. Coolant flow and curtain layer are both employed as the inlet boundary conditions with N_2 streaming at 4.5 m/sec at room temperature. In the computational model only three quarters of the fuel and oxidizer jets were simulated. LOX mass flow rate was 1.44 gm/sec at 100K. Gaseous Hydrogen streams in from the annular jets at 0.18 gm/sec. Temperature of H_2 at inlet was 200K. The LOX jet was modeled using EDP (Eulerian Dispersed Phase) mode in CFD++.

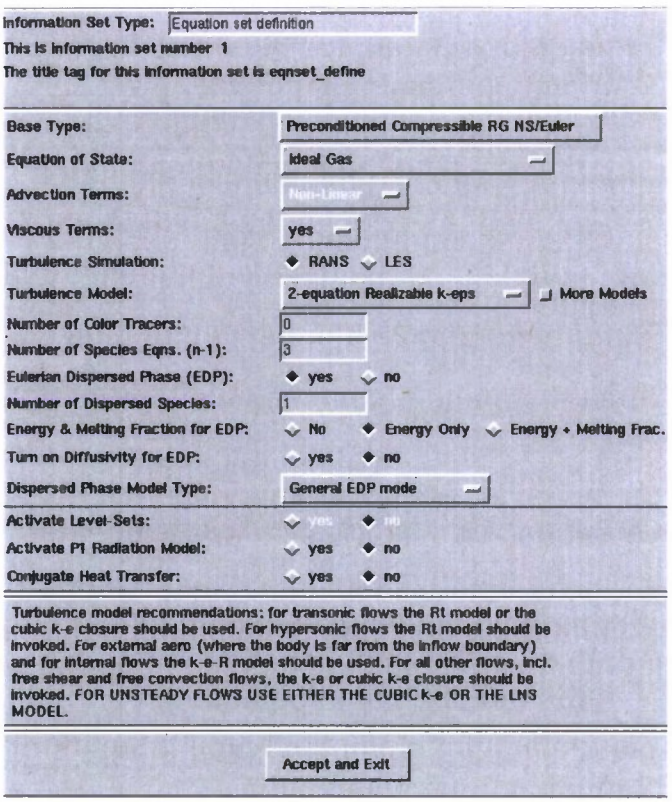

The figure shown above lists the equations chosen to simulate the flow. The two-equation k-epsilon model (RANS) was used. The carrier phase equations were solved using preconditioning to minimize numerical diffusion. The settings used in preconditioning the equation are shown in the following figure.

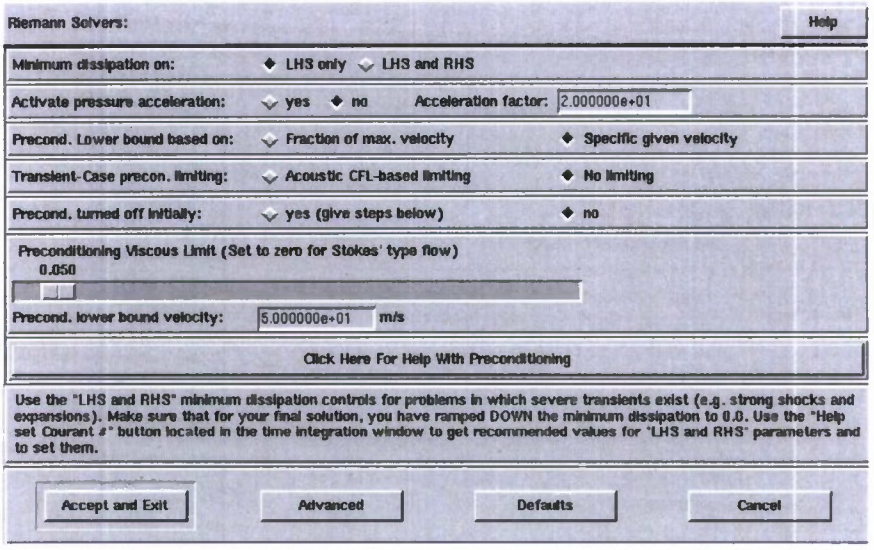

A simple one-step chemistry as shown below in the reactions window was employed.

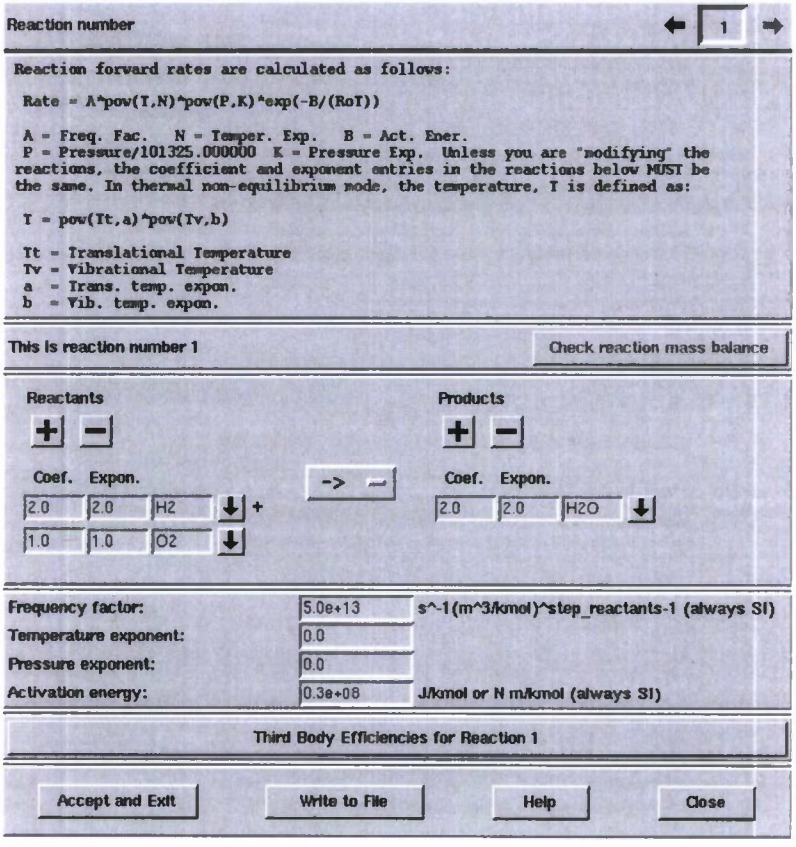

The options chosen to model the dispersed phase are shown in the following figures.

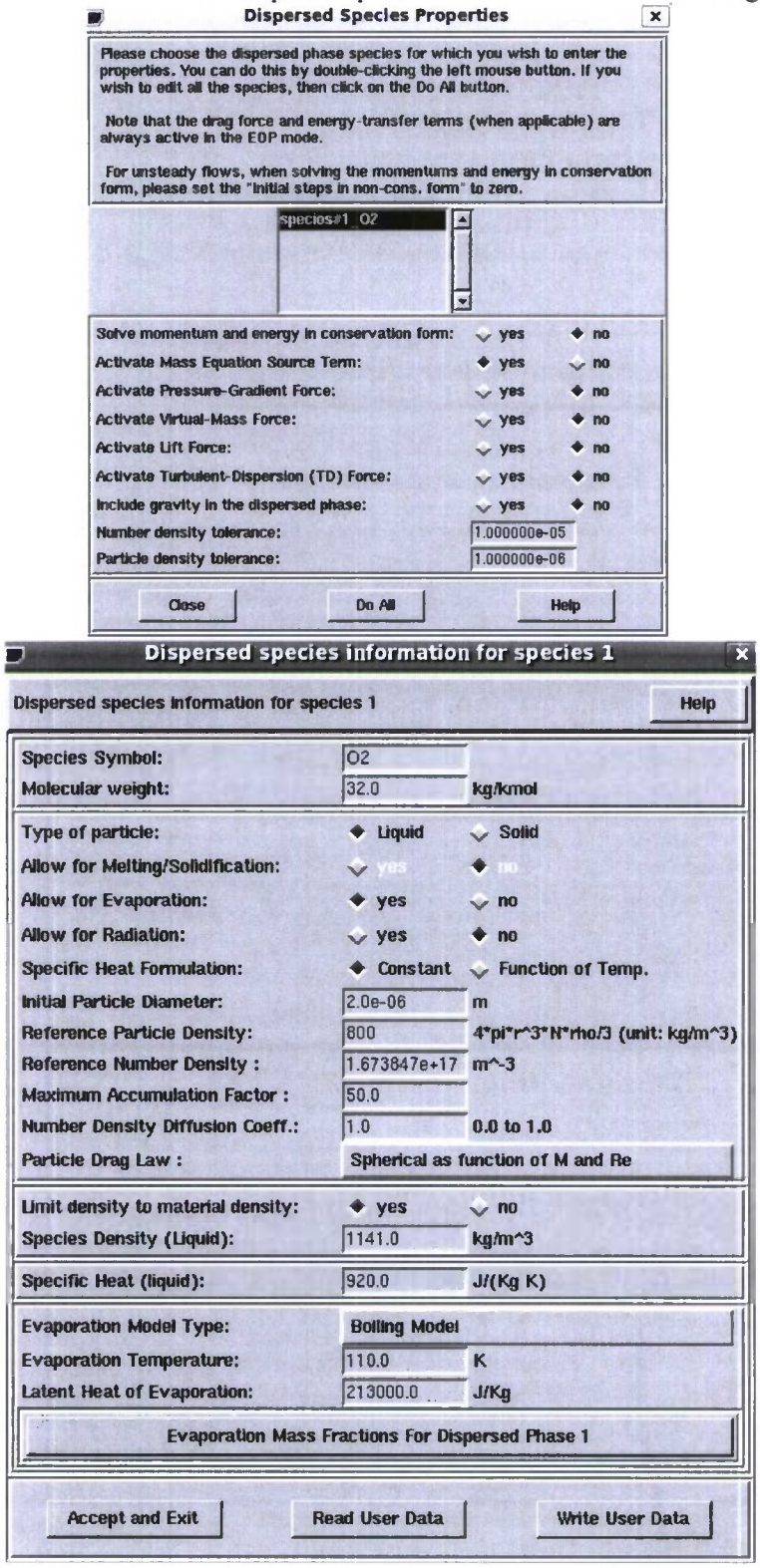

The following figure lists the boundary conditions used in the simulation.

1	Characteristics-based inflow/outflow	CURTAIN_LAYER
2	Characteristics-based inflow/outflow	FILM_COOL_LAYER
3	Symmetry	SYMMETRY1
4	Simple back pressure	OUTLET
5	Symmetry	SYMMETRY2
6	Multi-species inviscid surface tangency	INVISCID
7	Multi-species adiabatic wall function	WALL
8	Mass flow rate and temperature inflow	INNER_JET
9	Multi-species adiabatic wall function	INNER_JET_WALL
10	Multi-species adiabatic wall function	OUTER_JET_WALL
11	Mass flow rate and temperature inflow	ANNULUS_JET

The frozen flow field was initially setup. A heat source was then applied to the near-vicinity of the injectors to establish the flame. The heater was removed after the flame anchored itself. The time integration mode was switched to unsteady as shown in the following window and calculations were continued until residuals reached a plateau. The overall flux balance at this stage was within 1% of the inflow.

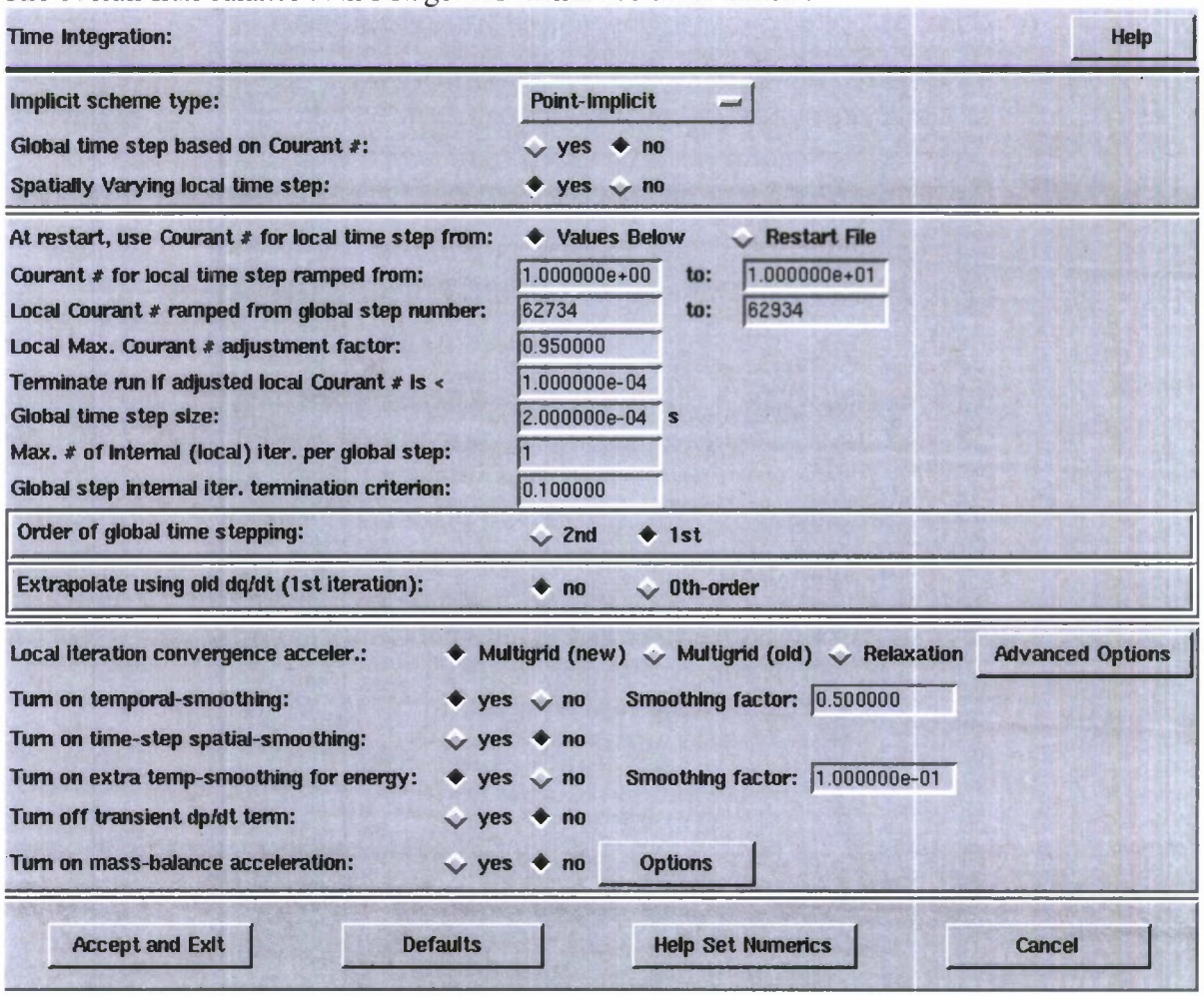

The next set of figures show the flow field at different streamwise locations. The labels on the contour slices are x locations in meters. The streamwise velocity distribution below shows the development of the shear layer between the fuel and oxidizer streams.

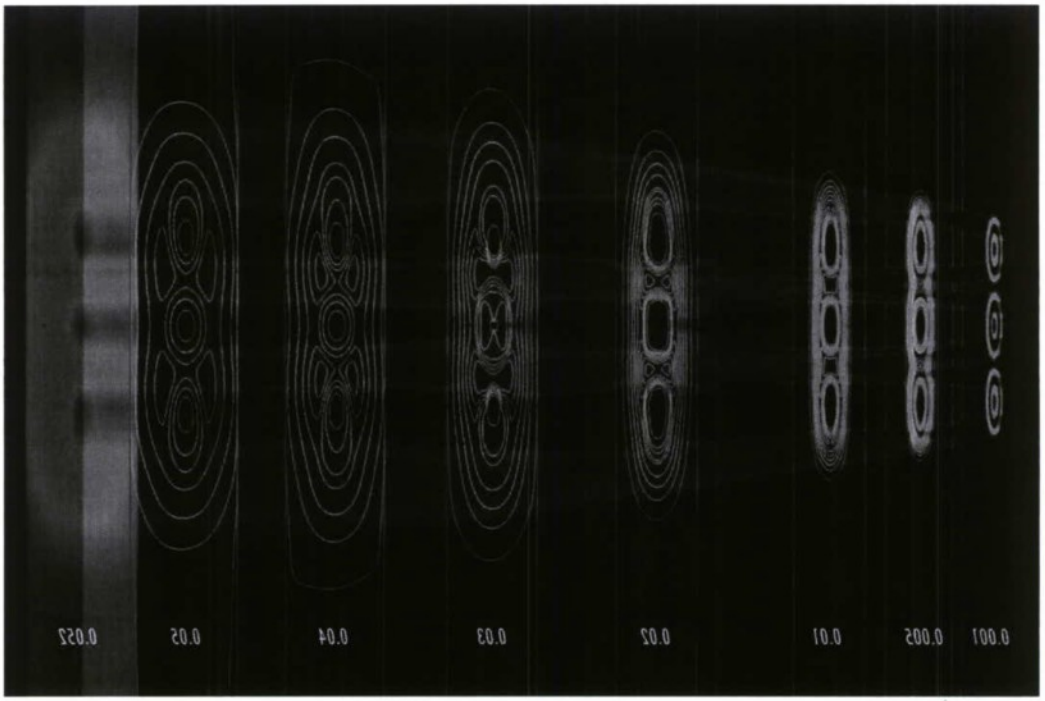

Gaseous O2 at the corresponding planes can be seen in the next figure. Almost 50 % of the O_2 fluxes out of the domain due to lack of gaseous fuel. The last plane in the following figure shows the amount of O_2 leaving the test section. Lack of complete combustion may be attributed to mixing of the fuel stream with the inert coolant stream.

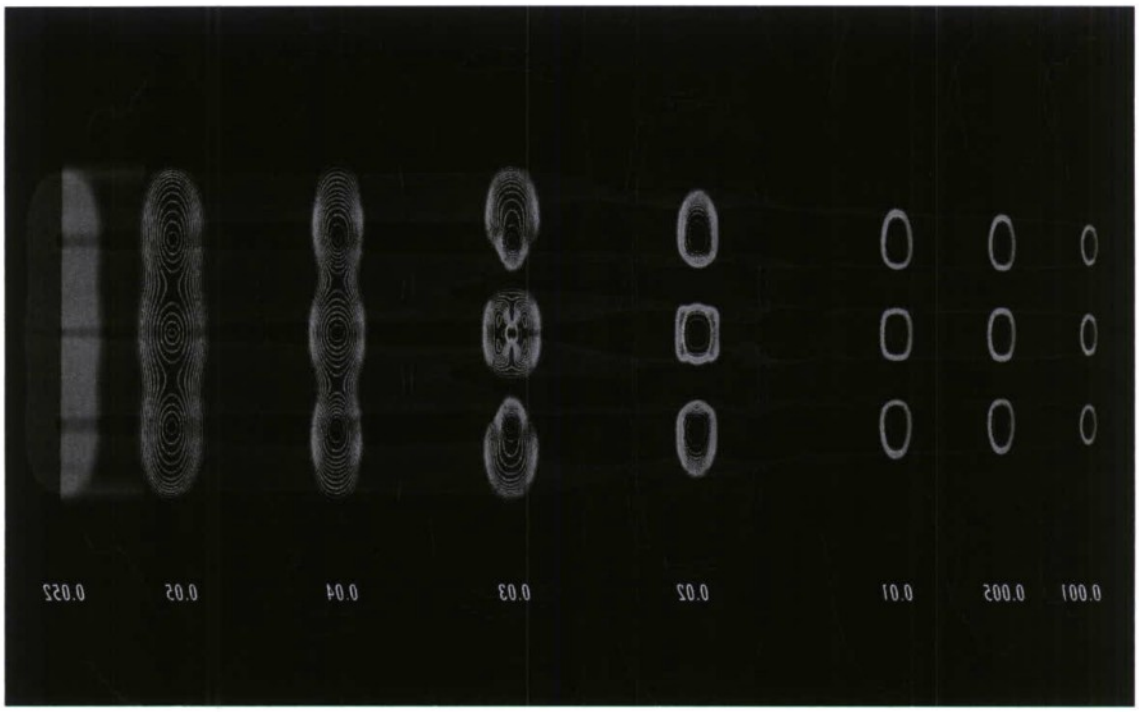

Hydrogen mass fractions (contour levels between 0 and 0.1) at the corresponding locations are shown below. About 50 % of H_2 spills in to the coolant stream and fluxes out of the domain unreacted.

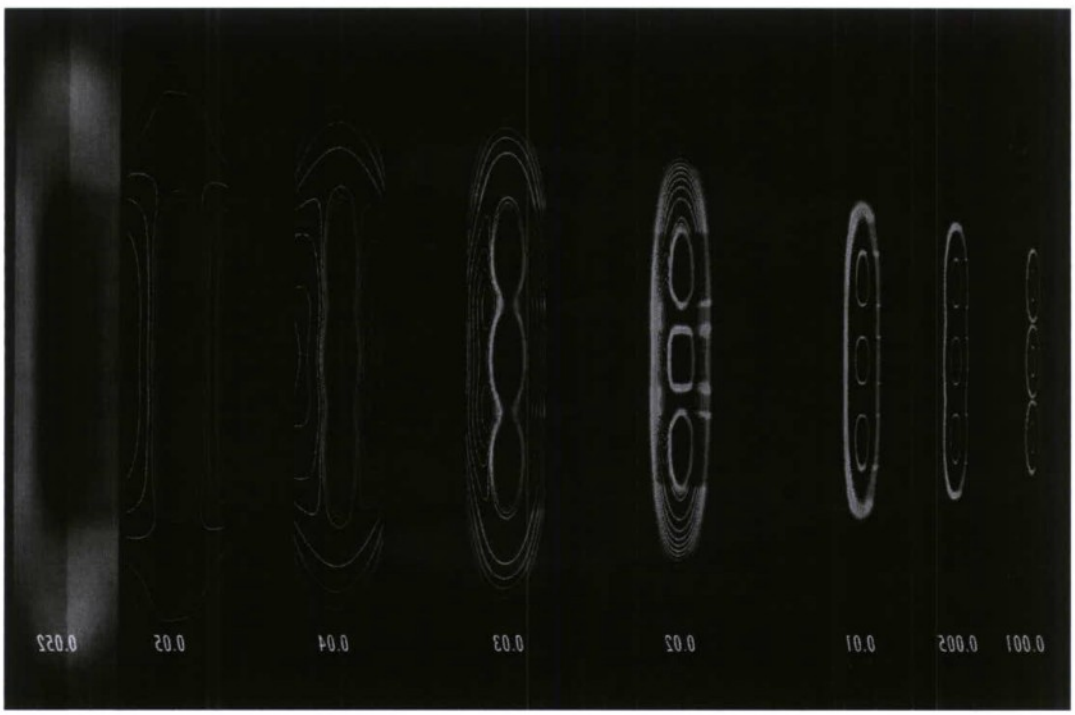

The next figure shows temperature contours. Flame location on the symmetry plane is also visible.

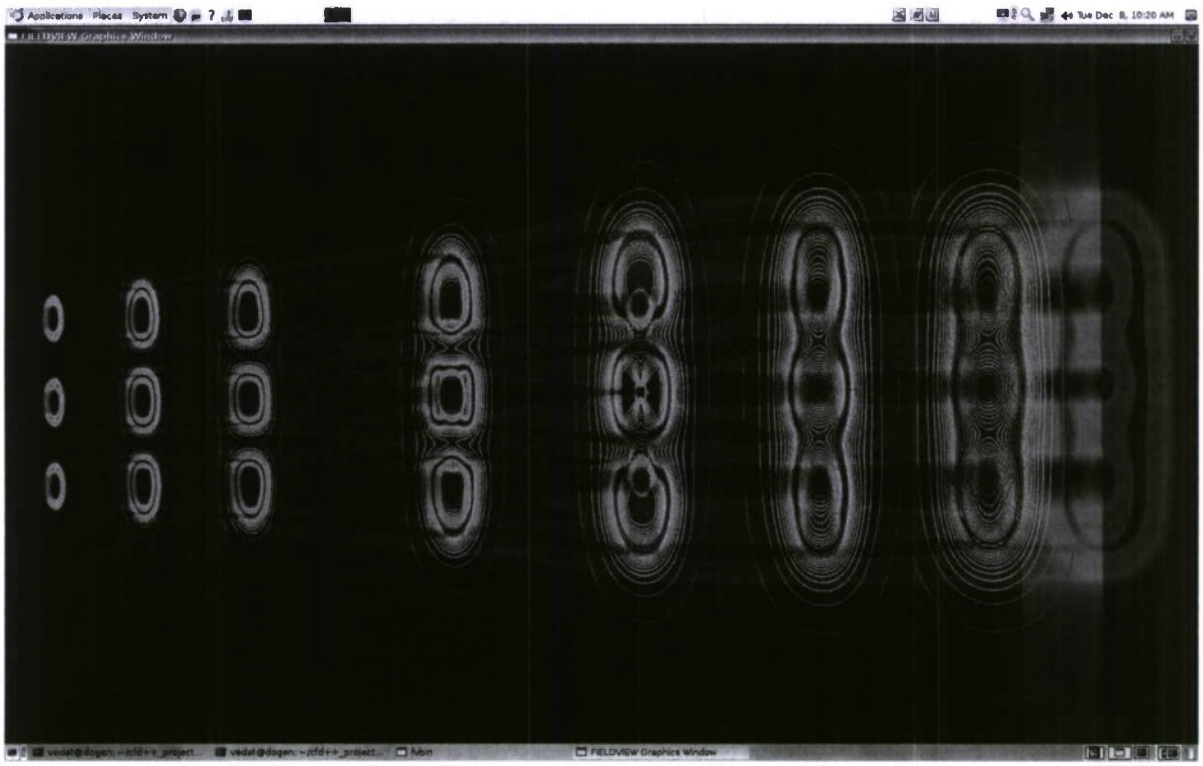

Temperature distribution on the wall is seen in the next figure. The wall temperature of almost 700 K is reached towards the exit of the domain. Adiabatic wall boundary

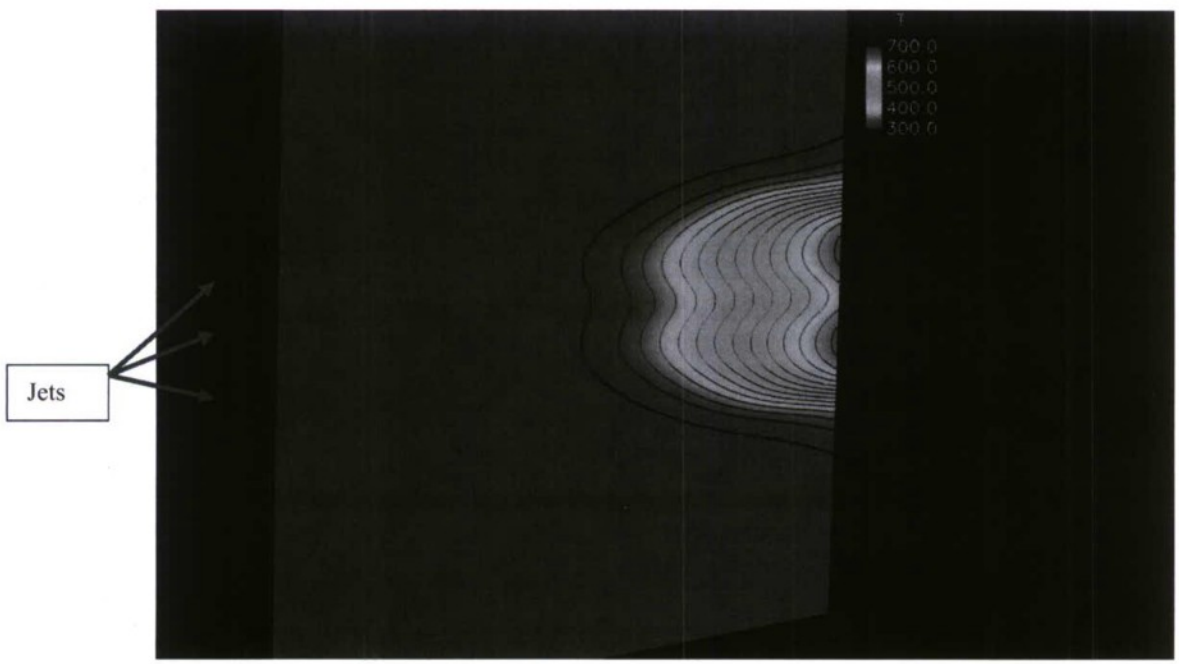

condition was used at the wall for this simulation in order to estimate the maximum temperature at the wall. The coolant inflow boundary was subdivided into two sections, one closer to the walls and the other surrounding the three jets. The next set of simulations will alter the inflow velocity in the region next to the wall to estimate the effect of coolant flow rate on maximum temperature at the wall.

A second case at higher chamber pressure produced higher wall temperatures as shown below. The maximum temperature increased to 1000 K at the wall. In this case flow remained unsteady and only an

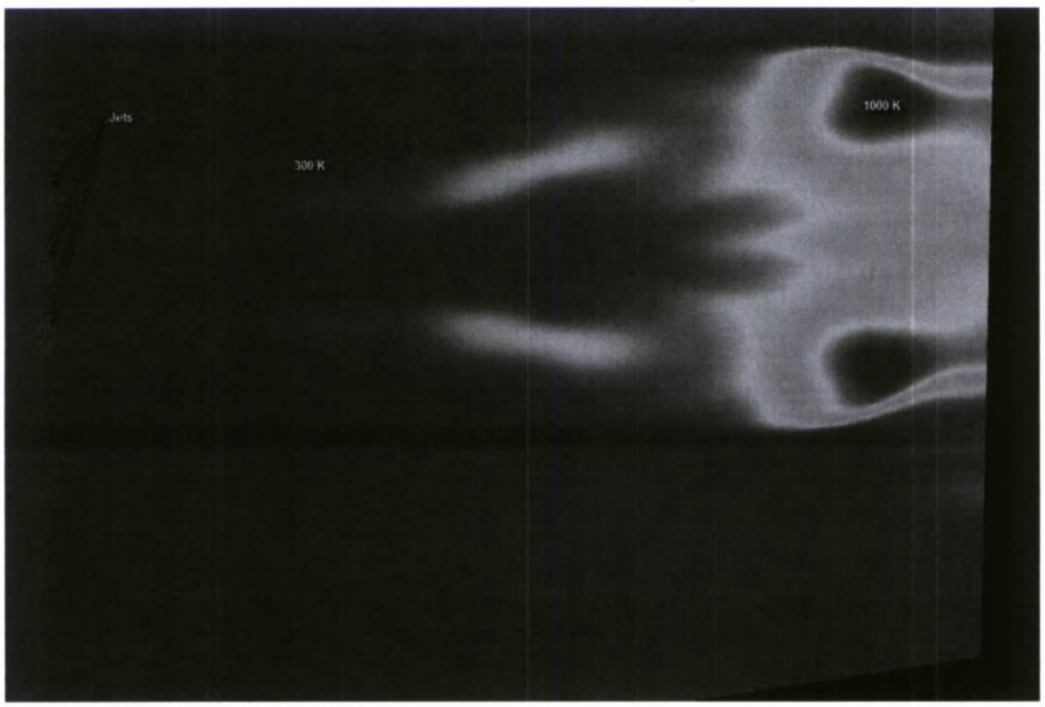

instantaneous snapshot is shown.

Conclusion

The capability in CFD++ to resolve acoustic oscillations and their coupling with reaction zones was improved. CFD++ can now resolve acoustic oscillations in combustion chambers. Acoustic modes were obtained for AFRL combustor stability test rig under quiescent conditions to study the impact of wave guide on the acoustic response of the fuel/oxidizer jets. Steady state calculations of the test facility are continuing to proceed in order to asses heat load on the wave guide for hot fire cases.

Effort and Accomplishments at Penn State University and Georgia Tech

Cryogenic Fluid Dynamic Response of Swirl Injector to External Forcing at Supercritical Conditions

This task extends our previous study on the eryogenie fluid dynamies of swirl injeetors at supereritieal eonditions to investigate the dynamic response of the injector to external excitations. The forcing is imposed through periodic oscillations of the mass flow rate at the injeetor tangential inlet over a wide range of frequencies relevant to the intrinsic flow instabilities of the injector.

The dynamic response of swirling jets to external excitations has been investigated by Panda and McLaughlin[1] using flow visualization teehniques. When the jet was exeited by acoustie oscillations with discrete frequencies in the upstream region, organized struetures evolved from the originally weak, irregular, and large-seale struetures under conditions without forcing. Cereedo *et al.*[2] found that when a eo-flow jet was foreed at its natural or sub-harmonie frequeneies, the turbulence properties were signifieantly ehanged. However, at the foreing frequeney twiee of the fundamental value, only modest influenee was observed. In the experimental study of Gallaire *et al.*[3], the vortex breakdown phenomenon was found unaffeeted by azimuthal foreing at the nozzle periphery since this proeess was governed by the dynamies in the eore region. Bazarov and Yang[4] developed a generalized linear theory on injeetor dynamies. Riehardson *et al.*[5] studied the dynamic response of a simple swirl injector using a boundary element method and compared the results with linear theory.

So far, very limited effort has been applied to study eryogenie fluid dynamies in a swirl injeetor using high-fidelity modeling and simulation teehniques, especially at conditions representative of liquid roeket operation. The present task is to develop a LES (large eddy simulation) based numerical framework within which various physical processes and flow parameters dictating the dynamic response of a eryogenie-fluid swirl injeetor can be studied systematieally. The theoretieal formulation and numerieal approaeh follow those reported in Zong and Yang.[6] The injeetor geometry and boundary eonditions are identical to the baseline ease of our previous study.[6] The mean mass flow rate is 0.15kg/s. External forcing is imposed by pulsating the mass flow rate at seleeted frequencies at the tangential inlet of the injector:

$$\dot{m} = \dot{m}_0 [1 + \alpha \sin(2\pi f_F t)] \qquad (1)$$

where $\dot{m}_0$ and f_F denote the mean mass flow rate and foreing frequeney, respectively, and α the oscillation magnitude, which is fixed to be 15%. The forcing frequency covers a range of 0.55-14 kHz, in order to eapture the broadband nature of the injeetor flow dynamics. Turbulenee with an intensity of 8% of the mean flow quantity is provided by super-imposing broadband noise onto the instantaneous mass flow rate.

Figures 1-2 show the temporal evolution of the temperature fields at foreing frequeneies of 14 kHz and 3.2 kHz, respeetively. The 14 kHz foreing does not show any signifieant

influenee on the flow dynamies. The wave strueture resembles that of the unforeed ease. Small disturbanees initiated in the upstream region grow as they are conveeted downstream. As noted in our previous study[6], the wave structure features three-dimensional hydrodynamie instability and propagates in a form similar to the shallow-water wave for an ineompressible flow. The high frequeney fluetuation deeays rapidly and disappears as the LOX film moves downstream due to viseous dissipation. Consequently, foreing at this frequeney does not affeet the flow field signifieantly. For the 3.2 kHz foreing ease, the wave structures on the LOX film lose their identities shortly after their appearanee. They breakup and merge into larger billows. The frequeney spectra of pressure fluetuation provide more quantitative insight into the various types of instability waves in the injeetor flow. Figures 3-5 indieate that the fluetuation magnitude at the foreing frequeney stands up in the bulk of the LOX film. In addition, foreing makes the power of other frequeney eomponents smaller and the frequeney eontent is reduced greatly, a situation eommonly known as the frequeney-locking phenomenon. Even the originally dominant fluetuation may lose most of its energy at some foreing frequencies.

Figures 6-9 show the variations of the mass flow rate at the injeetor inlet and exit for the eases with 3.2 kHz foreing and without oseillation. Foreing eauses the mass flow rate and film thiekness to vary in a more regular manner and the fluetuation magnitude of the spreading angle becomes larger. Figures 10-11 show the time-averaged film thickness and spreading angle as a funetion of foreing frequeney. The mean film thickness and spreading angle do not change much, due to eonservation of mass and momentum.

The injeetion dynamies ean be quantified globally in terms of the mass transfer funetion, defined as:

$$\Gamma_m(f)=\frac{\hat{m}^a_{ex}}{\hat{m}^a_{in}} \qquad (2)$$

where $\hat{m}^a$ is the Fourier component of the mass flow-rate fluetuation at the foreing frequeney. The subscripts *ex* and *in* denote the injeetor entranee and exit, respeetively. Figure 12 shows the magnitude of the injeetor mass transfer funetion as a funetion of the foreing frequeney. This quantity reaches its maximum around 1.9 kHz, eorresponding to the dominant frequeney of the intrinsie injeetor flow instability under the eondition without external foreing.

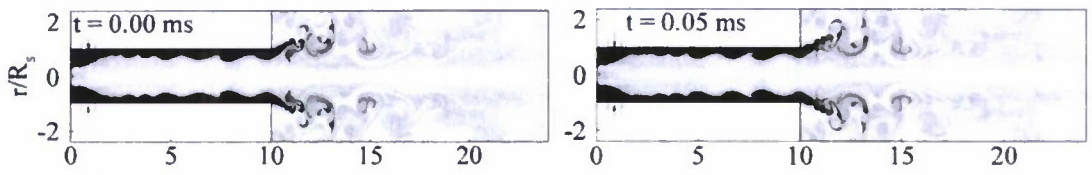

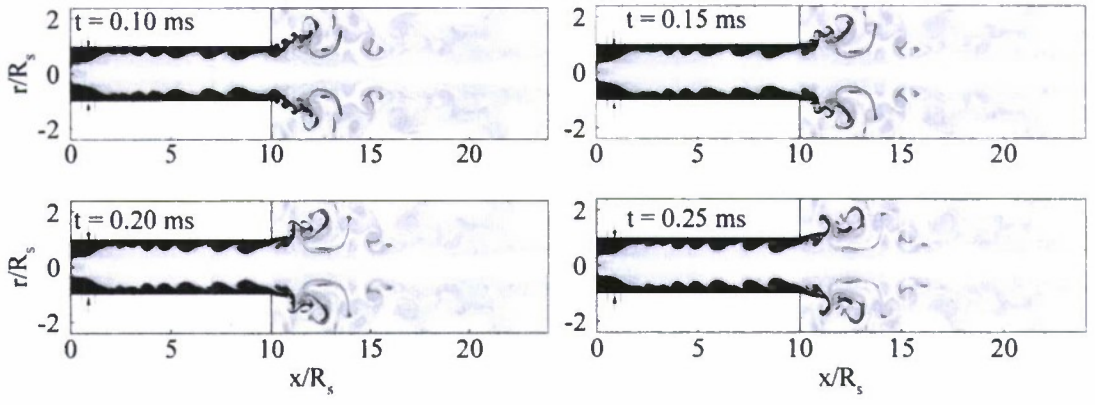

Figure 1. Temporal evolution of temperature field, external forcing at 14 kHz.

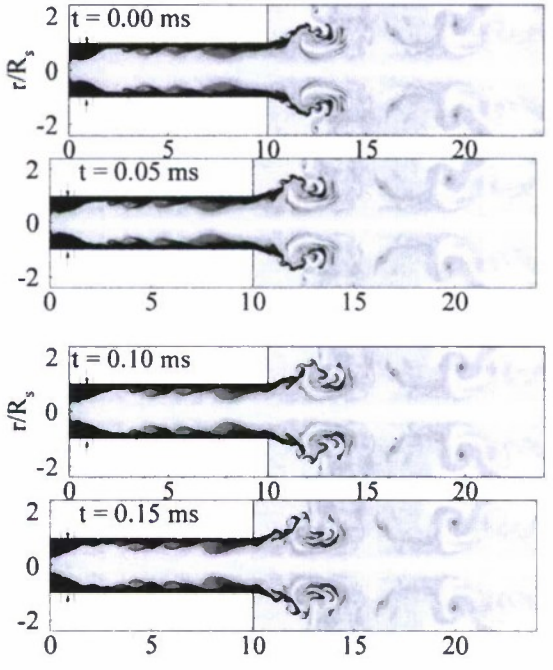

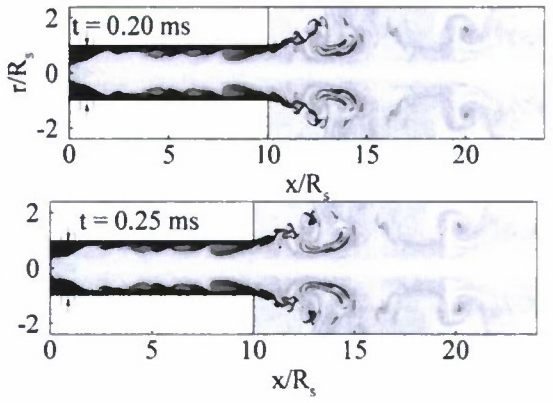

Figure 2. Temporal evolution of temperature field, external forcing at 3.2 kHz

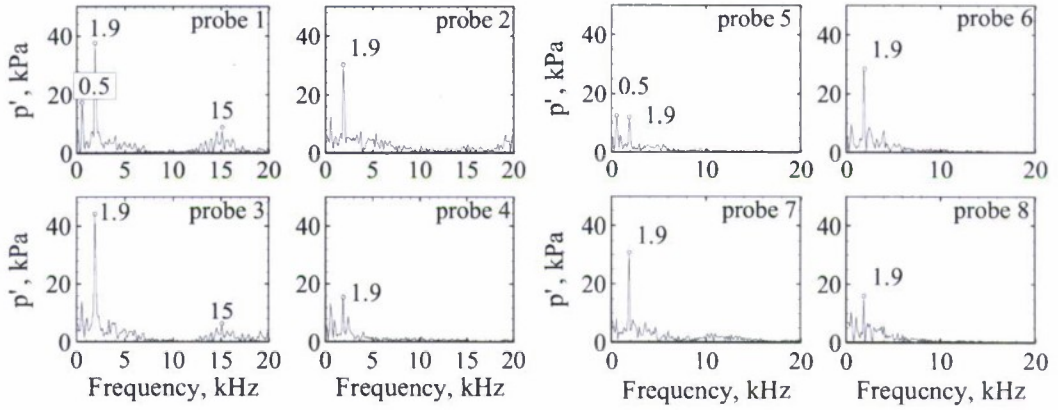

Figure 3. Power Spectral densities of pressure fluctuations at different locations inside injector, external forcing at 1.9 kHz

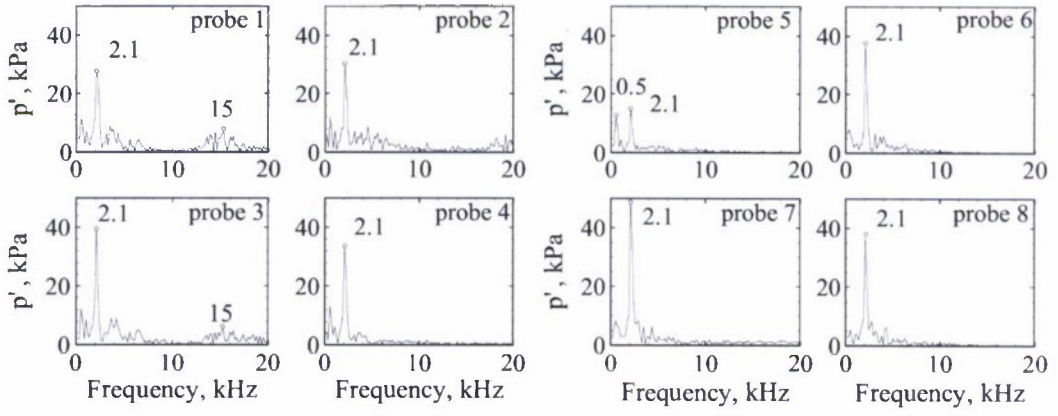

Figure 4. Power Spectral densities of pressure fluctuations at different locations inside injector, external forcing at 2.1 kHz

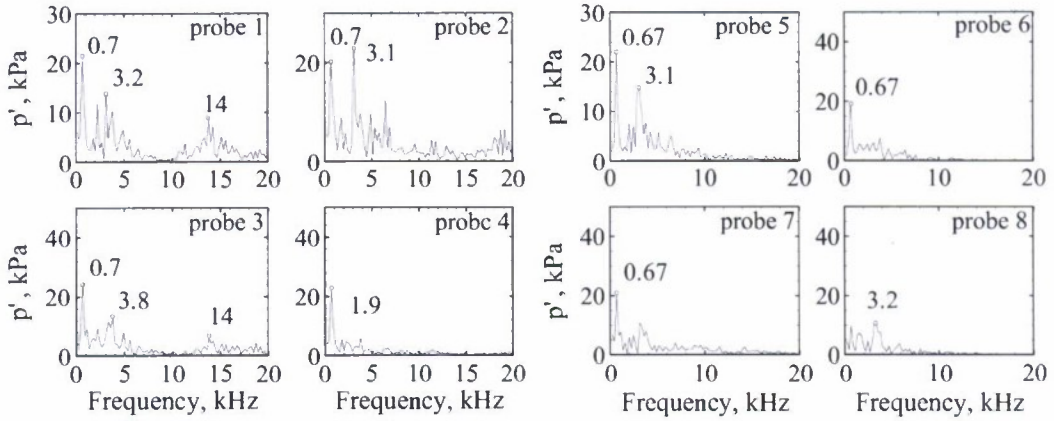

Figure 5. Power Speetral densities of pressure fluetuations at different loeations inside injeetor, external foreing at 3.2 kHz

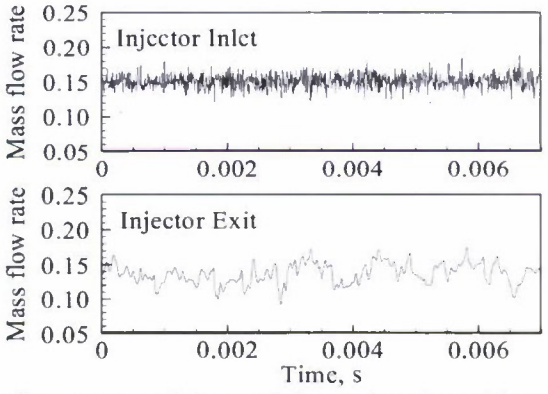

Figure 6. Mass flow rates at injeetor inlet and outlet without external foreing

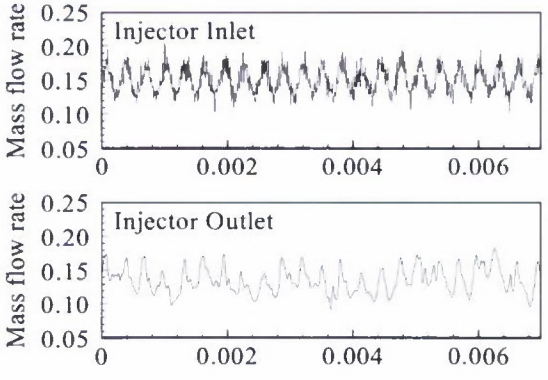

Figure 7. Mass flow rates at injeetor inlet and outlet with external foreing at 3.2 kHz

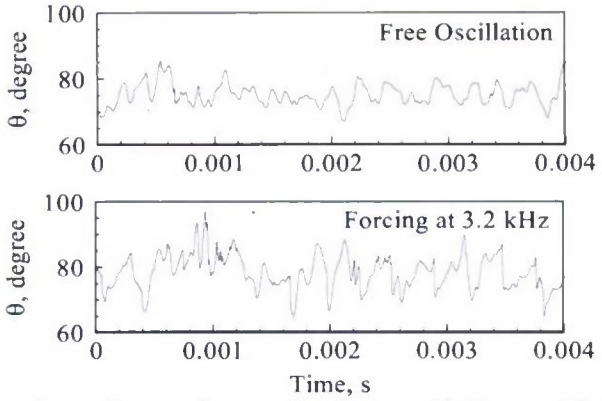

Figure 8. Comparison of spreading angle; free oscillation and 3.2 kHz forcing.

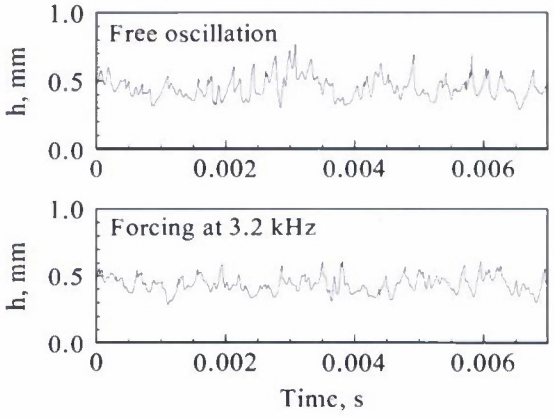

Figure 9. Comparison of injector exit film thickness; free oscillation and 3.2 kHz forcing.

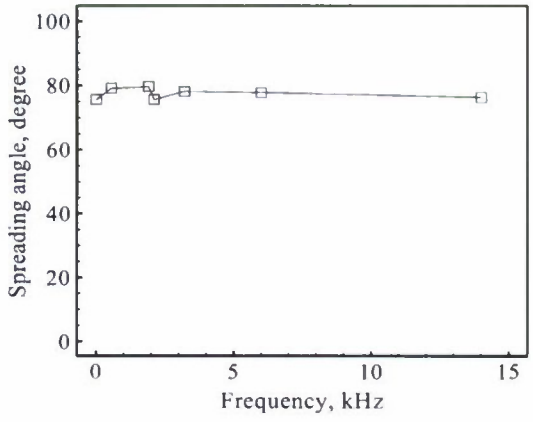

Figure 10.Variation of spreading angle with forcing frequency

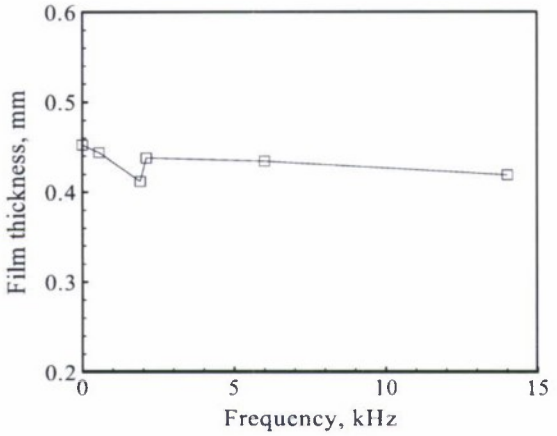

Figure 11. Variation of film thickness at injector exit with forcing frequency

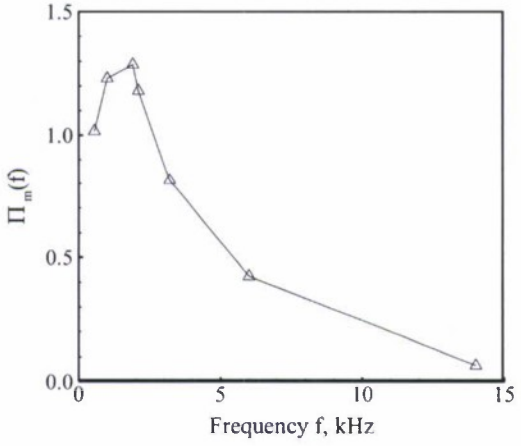

Figure 12. Frequency spectrum of magnitude of injector mass transfer function

REFERENCES

[1]Panda, J., and McLaughlin, D. K., "Experiments on the Instabilities of a Swirling Jet," *Physics of. Fluids*, Vol. 6, No. 1, Jan. 1994, pp 263-276.

[2]Cerecedo, L. M., Aisa, L., Garcia, J. A., and Santolaya, J. L., "Changes in a Coflowing Jet Structure Caused by Acoustic Forcing," *Experiments in Fluids,* Vol. 36, No. 6, Mar. 2004, pp. 867-878.

[3]Gallaric, F., Rott, S., and Chomaz, J.-M., "Experimental Study of a Free and Forced Swirling Jet," *Physics of Fluids*, Vol. 16, No. 8, Jul. 2004, pp. 2907-2917.

[4]Bazarov, V. G., and Yang, V., "Liquid-Propellant Rocket Engine Injector Dynamics," *Journal of Propulsion and Power*, Vol. 14, No. 5, Sept.-Oct., 1998, pp. 797-806.

[5]Richardson R., Park, H., Canino, J. V., and Heister S. D., "Nonlinear Dynamic Response Modeling of a Swirl Injector," AIAA Paper No. 2007-5454, 2007.

[6]Zong, N., and Yang, V., "Cryogenic Fluid Dynamics of Pressure Swirl Injectors at Supercritical Conditions," *Physics of Fluids,* Vol. 20, No. 5, May 2008, pp. 056103-1-056103-14.